

Multiple Paths to Enhance Optical Transmission through a Single Subwavelength Slit

F. J. García-Vidal,¹ H. J. Lezec,² T. W. Ebbesen,² and L. Martín-Moreno³

¹Departamento de Física Teórica de la Materia Condensada, Universidad Autónoma de Madrid, E-28049 Madrid, Spain

²ISIS, Université Louis Pasteur, 67000 Strasbourg, France

³Departamento de Física de la Materia Condensada, ICMA-CSIC, Universidad de Zaragoza, E-50009 Zaragoza, Spain
(Received 21 November 2002; published 29 May 2003)

In this Letter, we explore transmission properties of a single subwavelength slit flanked by a finite array of grooves made on a thick metallic film. We identify three main mechanisms that can enhance optical transmission: groove cavity mode excitation (controlled by the depth of the grooves), in-phase groove reemission (controlled by the period of the groove array), and slit waveguide mode (controlled by the thickness of the metal film). By tuning these geometrical parameters, enhancements of transmission of light by up to 2 orders of magnitude can be achieved when all three mechanisms coincide. Experimental verification of these findings is also shown for structured silver films fabricated by focused-ion-beam milling.

DOI: 10.1103/PhysRevLett.90.213901

PACS numbers: 42.25.Bs, 42.79.Ag, 78.66.Bz

Stimulated by the extraordinary optical transmission phenomena observed in 2D arrays of subwavelength holes [1], there is renewed interest in the optical properties of subwavelength slits perforated on metallic films [2–11]. One-dimensional arrays of very narrow slits have been theoretically analyzed and two types of transmission resonances were predicted [4,8]: coupled surface plasmon polariton (SPP) resonances and slit waveguide modes. Experimental verification of the existence of these transmission resonances has been reported in the microwave [5] and infrared [11] regimes. Very recently, it has been shown that enhanced transmission associated with the excitation of slit waveguide resonances is also present in single subwavelength slits [9,10].

In this Letter, we show both theoretically and experimentally that by corrugating a metal surface in the vicinity of a slit *two additional mechanisms* that also enhance optical transmission appear. More precisely, we study the transmittance of light passing through a metal film with a single slit, surrounded by a certain number of grooves. The grooves may be patterned either on the surface the light is impinging on (input corrugation, or IC), on the output surface (OC), or on both surfaces (IOC). In Fig. 1(a), we represent schematically single slit and IC configurations, showing the geometrical parameters defining the structures, as well as the coordinate axes used. Since in this Letter we try to provide a physical picture of the transmission mechanisms involved, we take all groove widths, depths, and first-neighbor distances between indentations (slit or grooves) to be equal, and we restrict ourselves to configurations that are symmetric with respect to the central slit plane of symmetry, denoting N_I (N_O) as the number of grooves to the right of the central slit at the input (output) surface. In this Letter, we present calculations for normal incident radiation of wavelength λ and p polarization [E field perpendicular to the grating symmetry plane, see Fig. 1(a)], polarization

for which enhanced transmission in an array of slits occurs.

First, we analyze the influence of patterning grooves on the input surface on T . Figure 2(a) shows the dependence of normalized-to-area transmittance, $T(\lambda)$, with N_I , for the IC configuration. We have chosen $d = 500$ nm, $h_1 = 100$ nm, $W = 350$ nm, and $a = 40$ nm. This set of parameters is typical for experimental studies in the

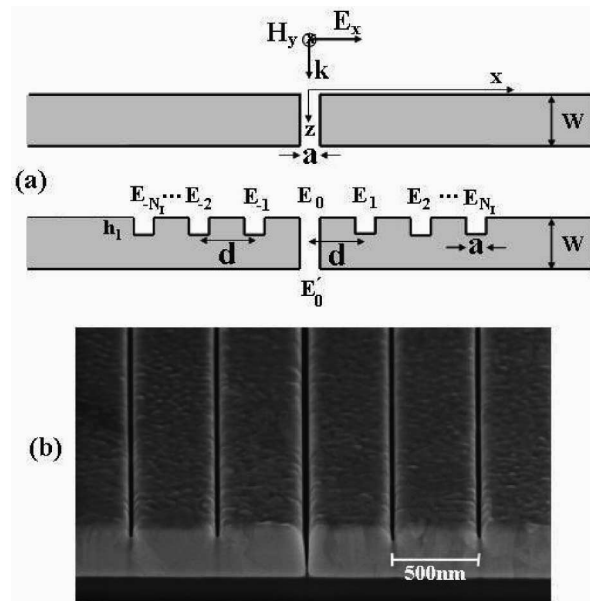


FIG. 1. (a) Schematic pictures of a single slit of width a in a metallic film of thickness W ; and IC: single slit symmetrically surrounded in the input surface by $2N_I$ grooves of depth h_1 . The separation between adjacent indentations is d and all groove widths are also a . A sketch of the p -polarized normal incident radiation is also shown. (b) Electron micrograph image of one of the devices analyzed and then cross sectioned by focused-ion-beam milling. Nominal values are $a = 40$ nm, $W = 350$ nm, $h_1 = 100$ nm, and $d = 500$ nm.

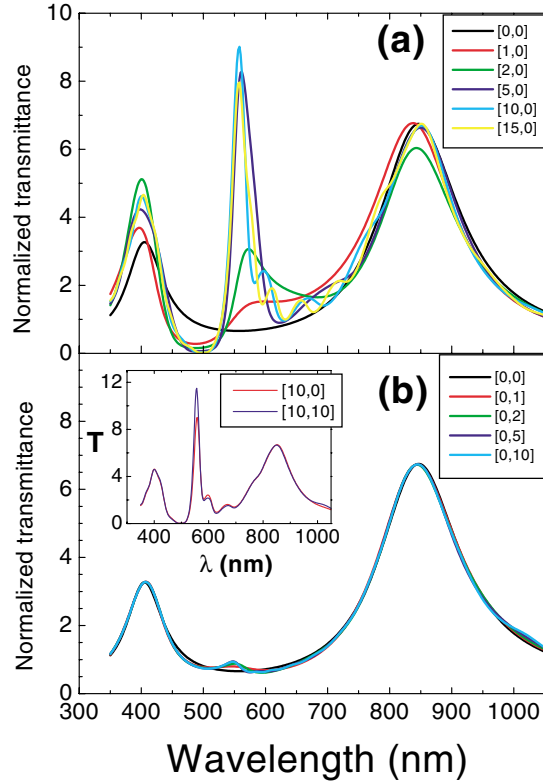


FIG. 2 (color). Normalized-to-area transmittance (see text) $T(\lambda)$, as a function of the number of grooves in (a) IC and (b) OC configurations. Geometrical parameters used in both figures are $a = 40$ nm, $d = 500$ nm, $W = 350$ nm, and the depth of the grooves $h_1 = h_2 = 100$ nm. Notation $[N_I, N_O]$ means $2N_I$ grooves in the input surface and $2N_O$ grooves in the output surface. In both surfaces, grooves are located symmetrically around the central slit. Inset of panel (b) shows $T(\lambda)$ for $[10,0]$ and $[10,10]$ configurations.

optical regime. The curve for $N_I = 0$ corresponds to the single slit case; in this frequency range, $T(\lambda)$ presents two maxima. It will be shown later that these two peaks are associated to the excitation of slit waveguide resonances. Figure 2(a) also shows that a maximum in $T(\lambda)$ develops at $\lambda_M \approx 560$ nm as N_I increases. This maximum is already apparent for $N_I = 1$ and, for this set of geometrical parameters, saturates at about $N_I = 5$, when T is enhanced by a factor of around 10.

Next, with respect to output corrugation, while it has been found [12,13] to strongly affect the angular distribution of transmitted light, producing highly collimated beams at resonant wavelengths, we show here that it has little effect on the total transmittance. This can be seen in Fig. 2(b), which shows $T(\lambda)$ for different N_O in OC configuration, and also in the inset of Fig. 2(b) showing that $T(\lambda)$ is quite similar for the IC and IOC configurations if they have the same N_I . In both cases, corrugating the output surface induces a change in $T(\lambda)$ of, at most, some 20%, again at wavelength λ_M .

As transmission is mainly governed by the structure of the input surface, we will further concentrate on the IC

configuration. Calculations were performed by considering perfect metal boundary conditions and a modal expansion of the EM fields [14]. In vacuum we expand the fields by a set of plane waves. For the grooves and central slit only the fundamental propagating eigenmode is considered, this is, for x inside indentation α [see Fig. 1(a)] the wavefield is a linear combination of $\phi_\alpha(x) \exp(\pm ikz)$, where $k = 2\pi/\lambda$ and $\phi_\alpha(x) = 1/\sqrt{a}$. Projecting the matching equation for E_x (at $z = 0$ and $z = W$) onto plane waves, the reflection and transmission coefficients can be expressed in terms of the wavefield inside the indentations. Additionally, H_y must be continuous at the indentation openings and $E_x = 0$ at the bottom of the grooves ($z = h_1$). This allows us to express all matching equations as a function of the set $\{E_\alpha, E'_0\}$, which give the x component of the electric field right at indentation openings: $E_x(z = 0^+) = \sum_\alpha E_\alpha \phi_\alpha(x)$ and $E_x(z = W^-) = E'_0 \phi_0(x)$. So, finally, after some straightforward algebra, we end up with the following set of $2N_I + 2$ equations for the unknowns $\{E_\alpha, E'_0\}$:

$$\begin{aligned} [G_{\alpha\alpha} - \epsilon_\alpha]E_\alpha + \sum_{\beta \neq \alpha} G_{\alpha\beta}E_\beta - G_\nu E'_0 \delta_{\alpha 0} &= I_\alpha, \\ [G_{00} - \epsilon_0]E'_0 - G_\nu E_0 &= 0, \end{aligned} \quad (1)$$

where α and β run from $-N_I$ to N_I .

These tight-binding-like equations remind us we are dealing with a resonant phenomenon, with I_α representing the “external illumination.” For a normal incident plane wave, and with the normalization we are using for $T(\lambda)$, $I_\alpha = 2$, for $\alpha = -N_I, \dots, N_I$. $G_{\alpha\beta}$ is the projection onto wavefields ϕ_α and ϕ_β ($G_{\alpha\beta} = \langle \phi_\alpha | G | \phi_\beta \rangle$) of the Green’s function: $G(\mathbf{r}, \mathbf{r}') = \frac{i\pi}{\lambda} H_0^{(1)}(k|\mathbf{r} - \mathbf{r}'|)$, $H_0^{(1)}$ being the Hankel function of the first kind. Then, the term $G_{\alpha\beta}E_\beta$ in Eq. (1) can be viewed as the illumination onto indentation α coming from indentation β . Indentation α is also coupled to the radiative modes of the vacuum regions and this is reflected in Eq. (1) by $G_{\alpha\alpha}E_\alpha$. $G_{\alpha\alpha}$ depends only on the ratio a/λ . In this system, both metal sides are connected only through the central slit by the term $G_\nu = 1/\sin(kW)$. Finally, ϵ_α reflects the back and forth bouncing of the EM fields inside indentation α : We find $\epsilon_\alpha = \cot(kh_1)$ for $\alpha \neq 0$ and $\epsilon_0 = \cot(kW)$. Once the values for E_α are calculated, the total transmittance can be obtained as $T = \text{Im}\{E_0 E_0'^*\} / \sin(kW)$.

From Eq. (1), we identify three different mechanisms that may enhance $T(\lambda)$. One mechanism already appears for a single slit. For this configuration, Eq. (1) gives $E_0 = 2(G_{00} - \epsilon_0)/D$ and $E'_0 = 2G_\nu/D$, where $D = (G_{00} - \epsilon_0)^2 - G_\nu^2$. Maxima in $T(\lambda)$ appear at wavelengths for which the denominator D is resonant. In the limit $a/\lambda \ll 1$, $G_{00} \ll 1$ and the maxima appear at $\lambda \approx 2W/n$, for integer n . These are the waveguide resonances associated to a slit with open ends that we discussed earlier.

Corrugating the input surface with grooves opens up the possibility for groove cavity modes, that would

provide large E_α for $G_{\alpha\alpha} - \epsilon_\alpha \approx 0$. For the case of very narrow square grooves, this condition is fulfilled for $\lambda \approx 4h_1/(2n+1)$, for integer n . Large E_α provide strong extra illumination into the central slit. Enhanced $T(\lambda)$ could be expected at groove cavity mode wavelengths. Actually, the situation is more complicated because, first, Eq. (1) must be solved self-consistently and, second, the illumination at the central slit depends on a weighted sum over all E_α , $\alpha \neq 0$, so care must be taken of phases from different contributions. From the asymptotic expression of $H_0^{(1)}(x)$ for large x , $G_{\alpha\beta} \approx \exp(ikd |\alpha - \beta|)$. All light reemitted from the grooves reaches the other grooves and the central slit in phase for $\lambda \approx d$. The combination of the two mechanisms (groove cavity mode and in-phase groove reemission) is responsible for the extra peak in transmittance shown in Fig. 2 at $\lambda \approx 560$ nm.

Figure 3 illustrates how the different mechanisms influence the transmittance, representing T versus both λ and groove depth, h_1 , for $W = 350$ nm and $d = 500$ nm. There are several regions where T is enhanced: the slit waveguide modes at $\lambda \approx 400$ nm and 850 nm, and the line that starts at $\lambda = d = 500$ nm for small h_1 going on as $\lambda \approx 4h_1$ for larger h_1 . By analyzing the homogeneous version of Eq. (1), it can be shown that this latter line corresponds to the excitation of a surface EM resonance of the corrugated input metal surface, originated by the interplay between the groove cavity mode and the in-phase groove reemission mechanisms. Additional insight into this surface resonance can be gained by considering what occurs in reflection gratings. Their absorption anomalies are also due to the excitation of surface resonances [15–17]. We have calculated the spectral positions of surface EM modes of a reflection grating with the same parameters as our finite structure and represented them in Fig. 3 (white dots). Figure 3 clearly shows that surface

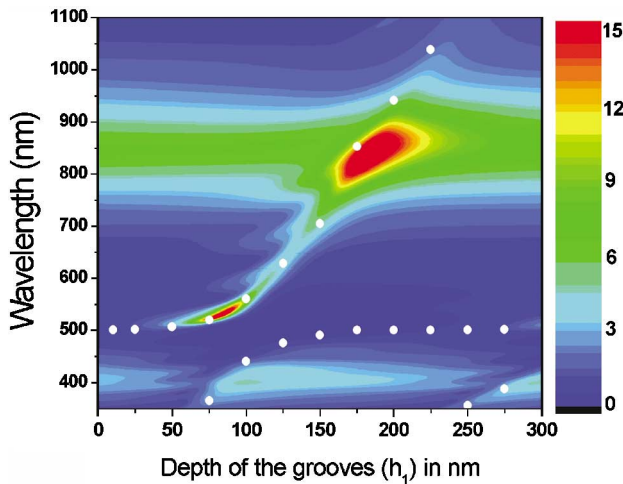


FIG. 3 (color). Contour plot of calculated transmittance vs both groove depth and wavelength, in IC configuration [10,0]. Here, $a = 40$ nm, $d = 500$ nm, and $W = 350$ nm. White dots correspond to the locations of surface EM modes of an infinite 1D array of rectangular grooves with different depths (h_1).

modes in reflection gratings originate from the anticrossing of two primary modes, each one of them associated with the two mechanisms described above. The fact that the transport anomalies of finite and infinite 1D arrays of grooves almost coincide shows that physical properties of corrugated metal surfaces are basically controlled by the local environment, as experimentally found [18]. Figure 3 also shows that the transmission is further enhanced when two mechanisms coincide. This is the case for $\lambda \approx 850$ nm, $h_1 \approx 175$ nm (coincidence of slit and grooves cavity resonances), and $\lambda \approx 525$ nm, $h_1 \approx 75$ nm (when the mixing of groove resonance and in-phase reemission is important). We note here that experimental evidence of enhanced transmission associated to the interplay between slit and groove cavity resonances has been recently reported in the microwave regime [19]. We predict a huge boost in T when *all three* mechanisms coincide. For example, for $W = 350$ nm and $N_I = 10$ as in Fig. 3, tuning both the in-phase condition (by choosing $d = 800$ nm) and the cavity mode resonance (by taking $h_1 = 150$ nm) to the 850 nm slit waveguide mode, we find that T is boosted by an additional factor of 10, reaching a value of $T \approx 150$, for $\lambda \approx 850$ nm.

In order to test these ideas, we have performed experiments in silver films (thickness $W = 350$ nm) evaporated on top of a quartz substrate. Many different devices were fabricated to study the dependence of their transmissive properties on the depth of the grooves and the period of the array. A focused-ion-beam (FEI DB235 system using Ga^+ ions, 5-nm nominal beam diameter) was used to mill a single slit surrounded by ± 5 grooves. Slit and grooves were 10 μm long, with a width $a = 40$ nm. Figure 4(a) shows (black curve and inset) the single slit $T(\lambda)$, which presents a broad maximum around $\lambda_{\text{SWG}} = 725$ nm. This maximum is due to transmission through a slit waveguide mode, when T is enhanced by a factor of about 6 with respect to the background. While calculations for perfect metals predict a background of $T \approx 1$ (see Fig. 2) for nonresonant transmission, the background T in silver films is always smaller. Also represented in Fig. 4(a) are the $T(\lambda)$ spectra when the slit is surrounded by grooves with a nominal depth $h_1 = 40$ nm, for different d . Under the presence of grooves, an additional transmission peak appears in the spectrum which, in keeping with the previous calculations, moves to longer wavelengths when d increases. This peak is strongest for $d = 650$ nm, when it appears at a wavelength λ_{SWG} , coinciding with the slit waveguide mode position. Once the optimal d has been found (for a given W , which determines λ_{SWG}), sweeping the groove depth provides the value that is optimal for transmission enhancement. This is represented in Fig. 4(b), which shows that the optimal groove depth is $h_1 = 40$ nm.

Calculations of transmittance spectra for a finite structure such as the one in case, using a realistic dielectric function, are a computational tour de force that are beyond our reach at the moment, which precludes a direct

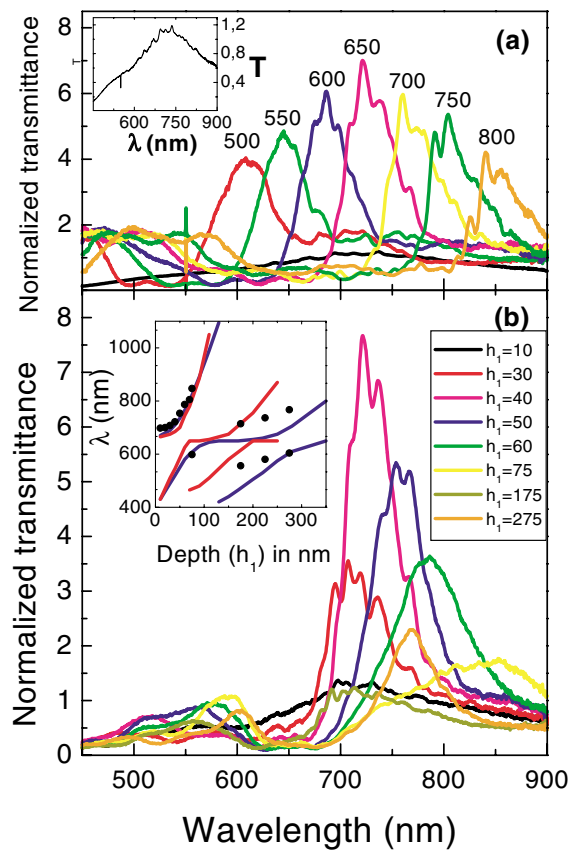


FIG. 4 (color). Collection of experimental $T(\lambda)$, for different structures formed by a central slit surrounded by ± 5 grooves ($a = 40$ nm) on the input surface of a silver film with $W = 350$ nm. (a) $h_1 = 40$ nm, while the array period (d) is varied between 500 and 800 nm. Black curve corresponds to the single slit case (also reproduced in the inset for clarity). (b) $d = 650$ nm, for different groove depths h_1 . In the inset, we compare the spectral locations of measured transmission peaks (black dots) with the calculated positions of the surface EM resonances of silver reflection gratings with square (blue curve) or triangular (red curve) grooves.

comparison with the presented experimental data. However, we can relate the transmittance peak positions to the computed wavelengths at which absorption anomalies occur in silver reflection gratings (calculations performed with the transfer matrix method [20] and using the dielectric function of silver taken from tables [21]). Cross sections of the experimental device show that the groove profile is triangular for small groove depths, and a more rectangular shape with a triangular tip for larger values of h_1 [see Fig. 1(b)]. The inset of Fig. 4(b) shows the measured wavelengths at which maximum transmission occurs as a function of h_1 (black dots) and the computed wavelengths of absorption anomalies in reflection gratings for both triangular grooves (red curve) and rectangular grooves (blue curve), showing a remarkable agreement. Notice, the crossover of the experimental values from the calculated for triangular grooves (for

small values of h_1), to the rectangular grooves (for large h_1), as expected from the cross-section studies.

We strongly believe that the analogs of the transmission mechanisms found in our 1D systems also play a crucial role in the process of extraordinary transmission recently reported for subwavelength holes surrounded by circular trenches [22].

In conclusion, we have studied the optical transmission properties of a single slit in a corrugated metal film. There are three mechanisms that enhance the transmission, which acquires a maximal boost when all three mechanisms collaborate, something that can be controlled with the geometrical parameters defining the device. Experiments have been carried out finding an optical transmission enhancement of a factor of 40 at triple coincidence. We have also shown that adding a grating to the output side does not “pull” more light through the slit (although it shapes the emerging radiation pattern [12,13]). We would like to stress here that, although we have focused in the optical regime, similar effects are expected for other electromagnetic ranges, once all dimensions are properly scaled.

- [1] T.W. Ebbesen *et al.*, Nature (London) **391**, 667 (1998); H.F. Ghaemi *et al.*, Phys. Rev. B **58**, 6779 (1998).
- [2] U. Schroter and D. Heitmann, Phys. Rev. B **58**, 15419 (1998).
- [3] M.M.J. Treacy, Appl. Phys. Lett. **75**, 606 (1999).
- [4] J.A. Porto, F.J. García-Vidal, and J.B. Pendry, Phys. Rev. Lett. **83**, 2845 (1999).
- [5] H.E. Went *et al.*, Appl. Phys. Lett. **77**, 2789 (2000).
- [6] E. Popov *et al.*, Phys. Rev. B **62**, 16100 (2000).
- [7] Q. Cao and Ph. Lalanne, Phys. Rev. Lett. **88**, 057403 (2002).
- [8] S. Collin *et al.*, Phys. Rev. B **63**, 033107 (2001).
- [9] Y. Takakura, Phys. Rev. Lett. **86**, 5601 (2001).
- [10] F. Yang and J.R. Sambles, Phys. Rev. Lett. **89**, 063901 (2002).
- [11] A. Barbara *et al.*, Phys. Rev. B **66**, 161403(R) (2002).
- [12] H.J. Lezec *et al.*, Science **297**, 820 (2002).
- [13] L. Martín-Moreno *et al.* Phys. Rev. Lett. **90**, 167401 (2003).
- [14] F.J. García-Vidal and L. Martín-Moreno, Phys. Rev. B **66**, 155412 (2002).
- [15] A. Hessel and A.A. Oliner, Appl. Opt. **4**, 1275 (1965).
- [16] R.A. Watts, T.W. Preist, and J.R. Sambles, Phys. Rev. Lett. **79**, 3978 (1997).
- [17] T. López-Ríos *et al.*, Phys. Rev. Lett. **81**, 665 (1998).
- [18] D.E. Grupp *et al.*, Adv. Mater. **11**, 860 (1999).
- [19] A.P. Hibbins, J.R. Sambles, and C.R. Lawrence, Appl. Phys. Lett. **81**, 4661 (2002).
- [20] J.B. Pendry and A. MacKinnon, Phys. Rev. Lett. **69**, 2772 (1992); P.M. Bell *et al.*, Comput. Phys. Commun. **85**, 306 (1995).
- [21] *Handbook of Optical Constants of Solids*, edited by E.D. Palik (Academic, Orlando, 1985).
- [22] T. Thio *et al.*, Opt. Lett. **26**, 1972 (2001).